Raman Spectroscopy as a Morphological Probe for TiO_2 Aerogels

Sean Kelly,[†] Fred H. Pollak,[†] and Micha Tomkiewicz*,[†]

Physics Department and the New York State Center for Advanced Technology in Ultrafast Photonic Materials and Applications, Brooklyn College of the City University of New York, Brooklyn, New York 11210

Received: September 9, 1996; In Final Form: November 16, 1996[⊗]

We report on the application of Raman scattering as a probe to follow the structural evolution of TiO_2 aerogels. We have traced the evolution of the 142 and 630 cm^{-1} E_g anatase peaks as a function of morphology. The results have been analyzed in terms of the q vector relaxation mechanism which predicts a unique relation between particle size and features of the Raman spectra. Since the phonon dispersion of anatase is not known, we have used the analogous rutile dispersion. There is good agreement between the particle sizes evaluated from the model and those determined by X-ray diffraction. Our results demonstrate that Raman spectroscopy can be an effective tool in monitoring the evolution of these aerogel systems.

Introduction

It is a pleasure to dedicate this article to the memory of Heinz Gerischer. We feel that this paper might be particularly appropriate since Heinz has dedicated significant effort to the understanding of the effects of particle size on the photocatalytic properties of semiconducting powders.[1−4] The main objective in these papers was to determine under what conditions the supply of oxygen will be rate limiting. However, his interest in the effects of size, structure, and morphology on the catalytic properties of semiconductors spans a major tread in his magnificent career.

It was demonstrated that every property of semiconducting photocatalysts is size dependent. These include optical properties,[5] dielectric constant,[6] mechanism of diffusion,[7] etc. All of these quantities apply to a collection of monodisperse single particles as well as to a collection of polydisperse particles. If in addition to defining the particle size distribution we can also specify the pore size distribution, the correlation between the morphology and functionality becomes a challenge.

Aerogels are arguably the simplest structures in which the fundamental building blocks are nanocrystallites so that the particle properties are associated with the properties of the nanocrystallites, yet the nanocrystallites are interconnected to form a well-defined pore structure. We have shown that TiO_2 aerogels are among the most efficient photocatalysts for oxidation of some organic substances.[8] We have also demonstrated that the quantum efficiency for photooxidation does not increase simply monotonically with the surface area but instead that there is optimal size distribution that implies a need to optimize morphology on more than one length scale.[9] This work was carried out under conditions in which diffusion of reactants or products is not rate limiting. One can expect that under different conditions, in particular under conditions in which diffusion is rate limiting, the morphological requirements will differ.

The morphology of the TiO_2 aerogels was characterized in terms of two length scales and three densities:[10] nanocrystallites of about 5 nm diameter close packed into 50 nm diameter mesoparticles that are loosely packed to produce ~80% porosity with surface area that can approach 1000 m^2/g. SEM and TEM photographs of those aerogels are also shown in ref 10. The TiO_2 aerogels were produced by sol−gel synthesis followed by supercritical drying. Since the sol−gel process involves a competition between hydrolysis and condensation that determines the overall structure and morphology,[11] it offers an excellent opportunity to optimize the morphology to achieve a desired functionality. In order to achieve this objective, one needs a probe that can follow the structural evolution from the early cluster formation, through the gelation process, and up to the final solid aerogel. Raman scattering is an excellent candidate to serve in this role. It has been demonstrated that the Raman scattering can be employed as a simple, rapid, and effective technique to evaluate nanocrystalline particle size.[12,15]

In this paper we present a Raman spectroscopic study of TiO_2 aerogels prepared through sol−gel synthesis followed by critical point drying and heat treatment. The details of the evolution of the Raman line shape (frequency shift, broadening, asymmetry) have been accounted for on the basis of the q vector relaxation model (QVRM). The effective particle sizes deduced from such an analysis are in good agreement with those found using X-ray diffraction.

Theoretical Background

For a perfect crystal, conservation of momentum requires that, in first-order Raman scattering, only optic phonons near the center of the Brillouin zone ($q \approx 0$) are involved.[12] In amorphous materials due to the lack of long-range order, the q vector selection rule does not apply, and the Raman scattering spectra will resemble the phonon density of states. Microcrystallites present an intermediate case where a range of q vectors, $\Delta q \approx 1/L$ (L is the particle size), are accessible due to the uncertainty principle.

The basic model due to the relaxation of the $q \approx 0$ selection rule for finite size crystals yields the following expression for the Raman intensity:[12,13]

$$I(\omega) \propto \int \mathrm{d}L\, \rho(L) \times \int_{\mathrm{BZ}} \exp(-q^2L^2/8) \frac{\mathrm{d}^3q}{[\omega - \omega(\vec{q})]^2 + [\Gamma_0/2]^2} \quad (1)$$

where $\rho(L)$ is the particle size distribution, q is expressed in units of π/a_L (a_L is the lattice constant), L is the particle size, $\omega(\vec{q})$ is the phonon dispersion, and Γ_0 is the intrinsic line

[†] Also at the Graduate School and University Center of the City University of New York, New York, NY 10036.

* To whom correspondence should be addressed.

[⊗] Abstract published in *Advance ACS Abstracts,* March 15, 1997.

S1089-5647(96)02747-2 CCC: $14.00

width. For analytical purposes the phonon dispersion curve in eq 1 is taken to be spherically symmetric and can be approximated by a simple linear chain model:[12]

$$\omega(q)^2 = A + \{A^2 - B[1 - \cos(qa)]\}^{1/2} \qquad (2)$$

The parameter A is related to the phonon frequency at the center of the BZ, and B determines the amount of the dispersion in ω. A positive (negative) value for the parameter B makes the dispersion negative (positive). For the case of a (negative, positive) dispersion eq 1 predicts an asymmetric (low frequency, high frequency) broadening and a (red shift, blue shift) of the peak with decreasing particle size. It should be noted that, in contrast to other mechanisms that could produce a shift and/or broadening of the Raman spectrum (e.g., strain[12]), eq 1 shows that with the QVRM there is a unique relation between particle size and the associated shift, broadening, and asymmetry (for a given dispersion). For nonuniform particle distributions, the broadening and the shifts will start to overlap, and one often resorts to empirical correlations. For example, the Raman intensity was found to increase approximately linearly with particle size.[14]

Arguably, the most comprehensive attempt to use Raman scattering as a probe to monitor the evolution of crystallinity from its chemical precursors to a translational invariant structure, on a system similar to the one of concern here, was published by Doss and Zallen[15] in their study of the sol−gel synthesis of alumina. In addition to our attempt to correlate the structural information to improve on the photocatalytic activity of the TiO_2 aerogels, we extend the Doss and Zallen methodology to a system in which the morphology was independently evaluated by a variety of techniques,[10] and the q relaxation mechanism is being evaluated quantitatively and not treated in a purely qualitative way. As in their case, the balance between broadening and peak shift due to the q vector relaxation and the particle distribution plays a key role in the analysis.

Experimental Section

Sample Preparation. The aerogels that we describe here were prepared by the following procedure:[8] TiO_2 sol was made containing 1 $Ti(O-C_3H_7)_4$:20 ethanol:4H_2O:0.08 HNO_3. Titanium isopropoxide $Ti(O-C_3H_7)_4$ (Alfa) was mixed with the anhydrous ethanol (analytical grade, Aldrich) at room temperature and added to a solution of ethanol + deionized water + 70% nitric acid over a 5 min period. The sol was stirred for an additional 5 min before transferring to plastic Petri dishes. The gels were then aged in alcohol for a few days to weeks before supercritical drying. The supercritical drying was carried out in a SAMDRI-790A (Tousimis) critical point dryer, which replaced the alcohol in the gel with carbon dioxide at the critical point of the carbon dioxide (35 °C and 1200 psi). The resulting aerogel has low density (0.5 g/cm^3) and a high porosity (80%). The samples were heated to different temperatures to produce various particle distributions.

Raman Scattering. The Raman measurements were made using the 514.5 nm line of an Ar ion laser as an excitation source. For the sol−gel samples the Raman scattered light was collected at 90° to the incoming laser light. For the aerogel samples the scattered light was collected in the in the back-scattering geometry. The laser power on the sample was about 3 W for the sol−gel samples and about 500 mW for the aerogel samples; no changes in line shape were noticed with variations in laser intensity. The instrumental resolution was about 3 cm^{-1} for the sol−gel samples and about 0.4 cm^{-1} for the aerogel samples. Light was detected with a CCD detector.

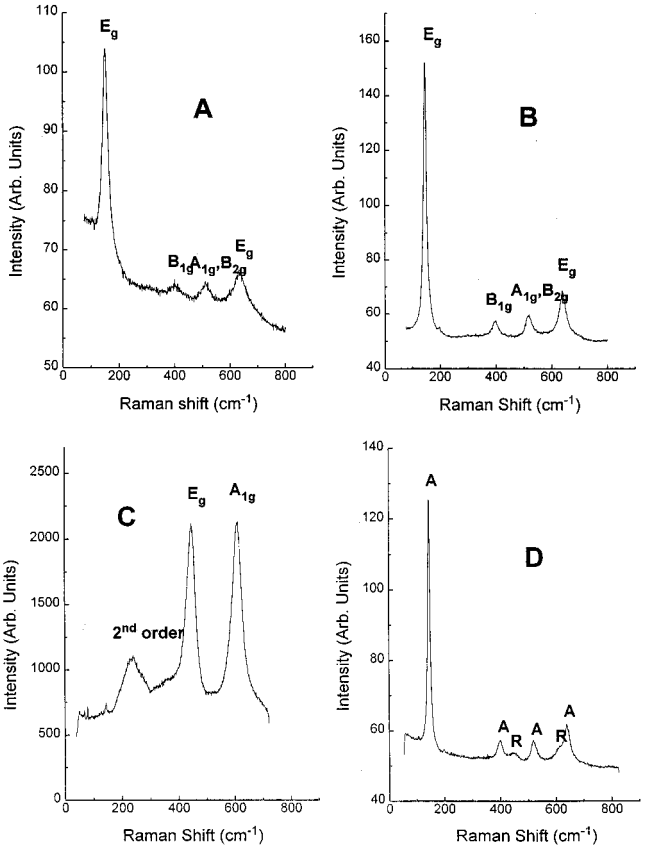

Figure 1. Raman spectra of TiO_2: (A) aerogel in anatase form after supercritical drying; (B) after heat treatment at 500 °C; (C) after heat treatment at 900 °C that converts it to rutile; (D) Degussa P-25 with a mixture of rutile and anatase phases.

X-ray Diffraction. The X-ray diffraction was carried out using a Rigaku diffractometer with a horizontal goniometer D/MAX-B. A Cu-sealed tube and a scintillation counter were used as the X-ray radiation source and the detector. The power settings of the source were 40 kV and 20 mA. The TiO_2 aerogel sample was grounded and mounted on an Al plate with a thin layer of silicon vacuum grease.

Results and Discussion

Figure 1 shows the Raman spectrum of the TiO_2 aerogels (A) before a heat treatment, after baking for 45 min at 500 °C that show only the anatase structure (B) and (C) after baking at 900 °C that transforms the crystalline structure from anatase to rutile.[16] We show in this figure also the symmetry designations of the various features.[17] For comparison, Figure 1D shows the Raman spectrum of Degussa P-25 powder in which a mixture of anatase and rutile can be observed. Figure 2 shows a comparison of the (A) 142 cm^{-1} E_g and the (B) 630 cm^{-1} E_g peaks of an aerogel with small crystallites (solid line) to one with large crystallites (dotted line). It summarizes the main experimental observations that are associated with changes in the particle size: with a decrease in particle size the peak broadens asymmetrically (high frequency), shifts to the blue, and decreases in intensity. These effects are much more pronounced for the 142 cm^{-1} spectrum.

For this study, the main tool that we have used to change the morphology and the particle size distributions was thermal annealing after the supercritical drying. Figure 3 shows the shift in peak position of the 142 cm^{-1} (solid circles) and the 630 cm^{-1} (open squares) peaks as a function of the X-ray diffraction crystallite size. Figure 4 shows the corresponding FWHM

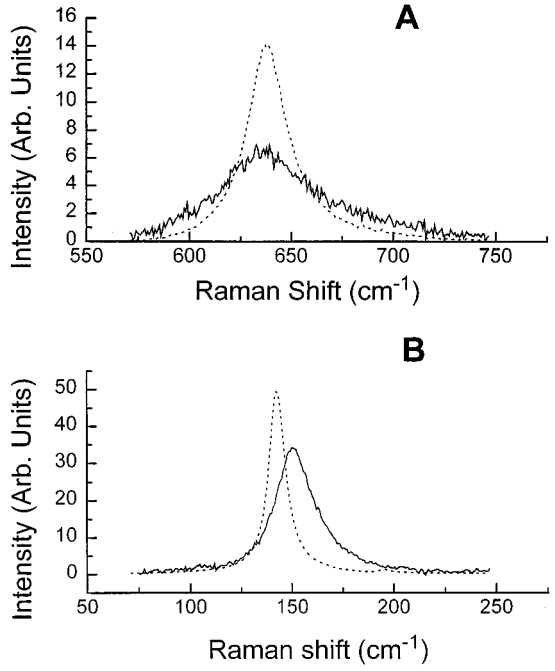

Figure 2. Comparison of the 630 cm^{-1} peak (A) and the 142 cm^{-1} E_g peaks (B) of an aerogel with small crystallites and large crystallites.

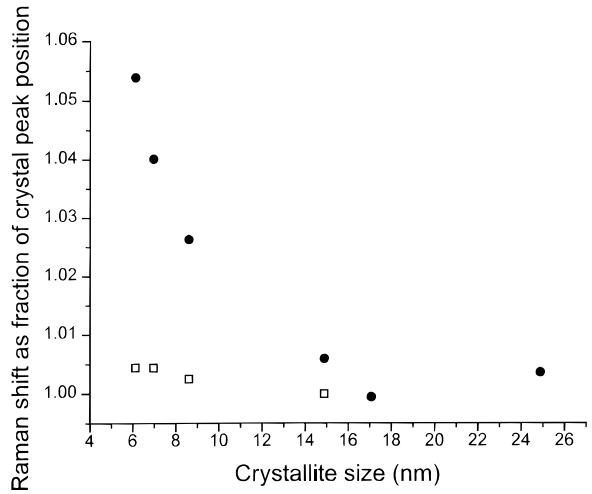

Figure 3. Line shifts of the 142 cm^{-1} (●) and the 630 cm^{-1} (□) peaks with the corresponding X-ray diffraction crystal size.

versus crystallite size. Figure 5 shows the evolution of the 630 cm^{-1} peak during the sol condensation. This peak is the dominant peak in the sol and gel phases (after subtracting the solvent lines). We do not have an exact assignment for this line; however, a 665 cm^{-1} line was associated by Best and Condrate in their investigation of SiO_2-TiO_2 glasses,[18] with the octahedrally coordinated Ti. Figure 6 shows the correlation between the peak width and peak shift. In terms of fractional changes from the corresponding large crystallite values. This correlation was previously empirically correlated[15] with the nature of the particle network.

Figure 7 shows a simulation of the 142 cm^{-1} peak using eq 1 for two values of L, i.e., $6a_L$ and $10a_L$, where a_L is the length of the crystal unit cell in eq 1. The nature of $\omega(\vec{q})$ used in this calculation is discussed below. One thing to note is that for anatase the unit cell has dimensions $3.79 \times 3.79 \times 9.51$ Å. For simplicity, we have taken the phonon dispersion to be spherically symmetric. The parameter a_L in the simulation will be an "effective" unit cell length, which we predict to lie between 3.79 and 9.51 Å. A second problem we have is that the phonon

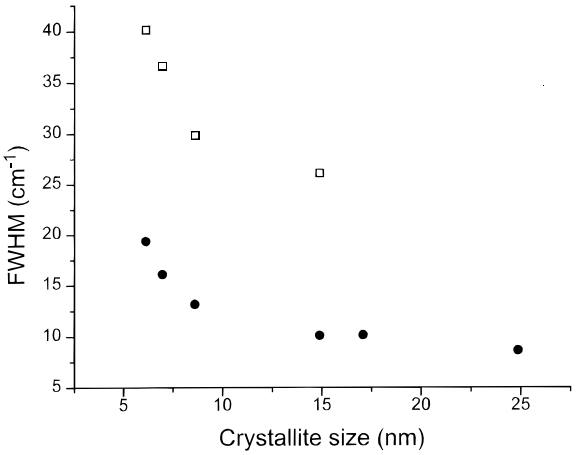

Figure 4. Line widths of the 142 cm^{-1} (●) and the 630 cm^{-1} (□) peaks with the corresponding X-ray diffraction crystal size.

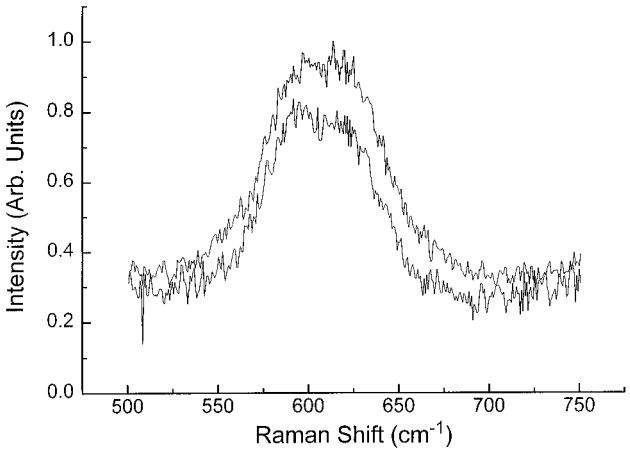

Figure 5. Evolution of the 600 cm^{-1} peak during the sol formation. The lower peak was taken 1 min after mixing of the reactants while the upper peak was taken 275 min after mixing (almost gel).

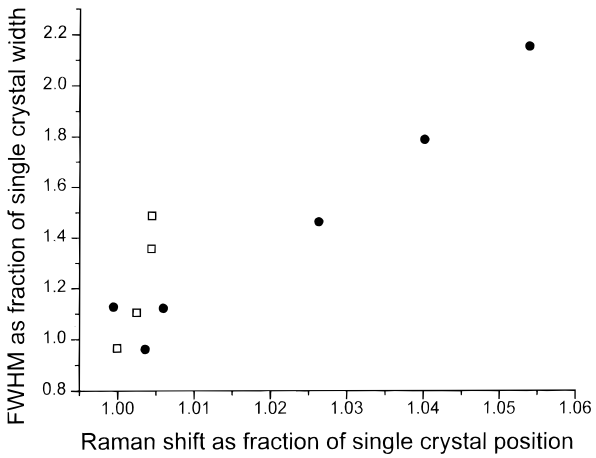

Figure 6. Correlation between the fwhm and peak shift of the 142 cm^{-1} (●) and the 630 cm^{-1} (□) peaks. The fwhm and the shifts are given as fractional changes from the large crystalline values.

curves for anatase have never been measured. When large enough crystals of anatase can finally be grown, neutron scattering will allow the measurement of the phonon dispersion curves. Some ab initio calculations have been done for anatase, and for the 142 cm^{-1} E_g peak the phonon mode is similar to that of the rutile mode Γ_{3+}.[19] Examining the phonon dispersion curve originating at 142 cm^{-1} for rutile reveals that it has a positive dispersion, and the BZ edge is about 80% higher than at the center of the BZ.[20] The simulation in Figure 7 was

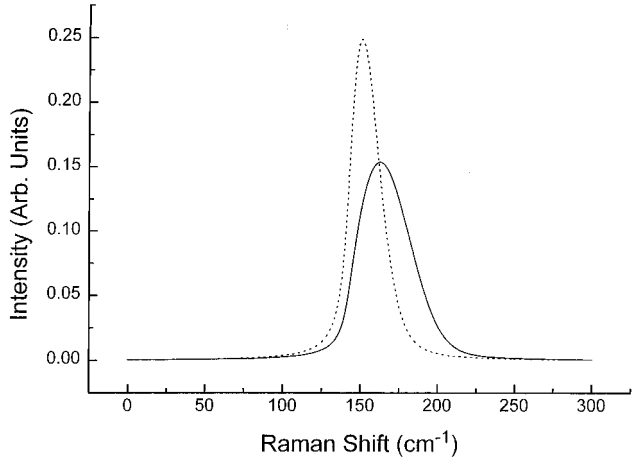

Figure 7. Simulation of the 142 cm^{-1} peak using eq 1 for two different crystalline sizes: (—)6_{aL}, (- - -) $10a_L$.

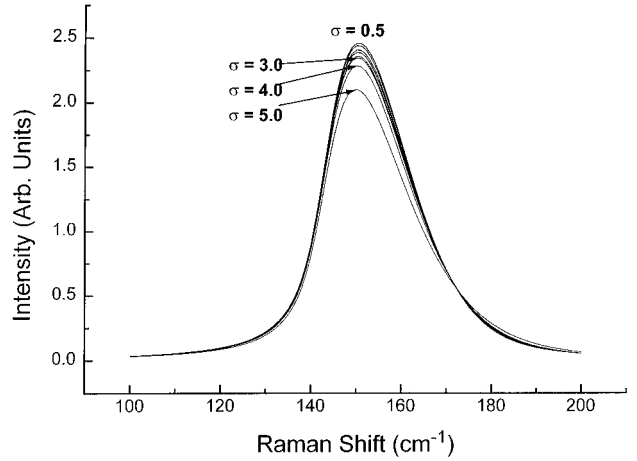

Figure 8. Simulation of the 142 cm^{-1} peak using eq 1 with a Gaussian particle distribution with a mean of $10a_L$ and different standard deviations.

performed with an 80% positive dispersion. The shift, broadening, and intensity follow the experimental results. The peak shift and broadening are uniquely interrelated through the particle size distribution.[15] The particle distribution of the TiO_2 aerogels was previously described.[10] The nanocrystallites approximately follow a narrow Gaussian distribution with a mean of about 2.2 nm and σ of about 0.8 nm. Figures 8 and 9 show the effects of the widths of the distribution for distribution means of $10a_L$ and $30a_L$. These curves were simulated with the same positive dispersion as the one described previously. One can see a small red shift with widening of the particle distribution in the $10a_L$ mean. There is no detectable shift in the peak position for the $30a_L$ mean. Similar to the conclusion in ref 15, the widening of the distribution and the q relaxation mechanism shift the spectra in opposite directions. However, the shift due to the widening of the distribution is considerably smaller compared to that of the QVRM. This difference was used in ref 15 to suggest that the small shift in the sol−gel phase corresponds to a wide particle size distribution while the corresponding changes in the solid correspond mainly to the QVRM. It is obvious that both mechanisms contribute throughout; however, the uncertainty with the dispersion precludes deconvolution of these two effects.

Figures 10 and 11 summarize the results: They show the theoretical FWHM and position of the 142 cm^{-1} peak superimposed with the experimental data, as a function of crystallite size. While the experimental crystalline size was determined from X-ray crystallography, the theoretical fits were presented

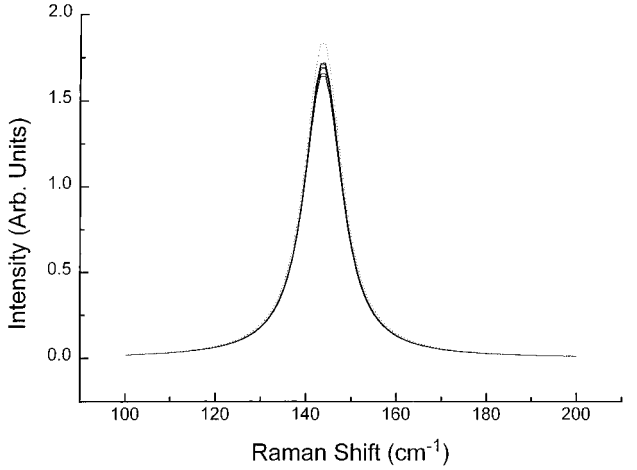

Figure 9. Simulation of the 142 cm^{-1} peak using eq 1 with a Gaussian particle distribution with a mean of $30a_L$ and different standard deviations.

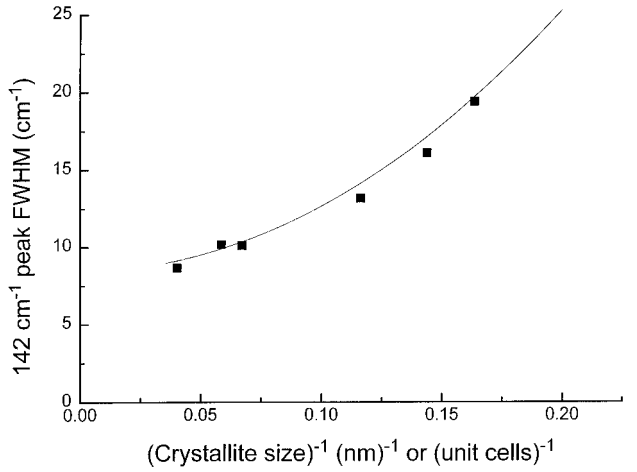

Figure 10. Correlations of the crystallite size and the line widths of the 142 cm^{-1} peak: (—) theory, (■) experiment.

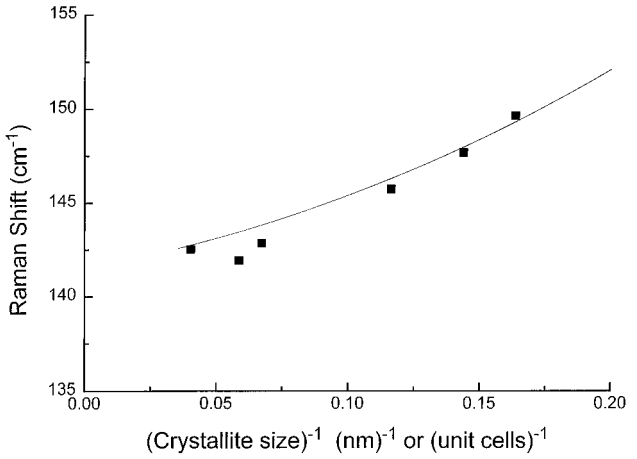

Figure 11. Correlations of the crystallite size and the peaks position of the 142 cm^{-1} peak: (—) theory, (■) experiment.

in terms of multiples of unit cell size. The scaling of the "effective" unit cell size was done so that the slopes of the theoretical and experimental data in Figure 10 will agree. The data in Figure 11 were drawn without any adjustable parameters. This scaling produced "effective" unit cell size of 5.55 Å for the 80% positive dispersion. If we examine the weighted average for the dimensions of the anatase unit cell, we calculate a value of 5.70 Å. There is extremely good agreement between the calculated "effective unit cell" and the weighted average

anatase unit cell dimensions. Using Figures 10 and 11, one can fit the data to expressions of the type[15]

$$\Delta\omega = k_1(1/L^{\alpha}) \quad (3)$$

$$\Gamma = k_2(1/L^{\alpha}) + \Gamma_0 \quad (4)$$

where $\Delta\omega$ is the shift and Γ is the line width. α is a scaling parameter that was related to the network structure. It was found that for materials with layer structure such as graphite and boehmite α is $\approx$1 while for covalently bonded semiconductors such as Si and GaAs α is $\approx$1.5. From Figure 10 α is found to be 1.55.

Conclusions

We have shown that for the case of anatase TiO_2 aerogels the details (shift, broadening, and asymmetry) of the Raman spectra of the 142 cm^{-1} feature can be described quite well using the QVRM with a positive dispersion of 80%. The "effective" mean size of the crystallites corresponds precisely to that of X-ray diffraction. Raman spectroscopy can also aid in understanding the morphology during the sol−gel stage as we have shown that a more likely explanation for the small changes in Raman line position and broadening are due to differences in the particle distribution than to the QVRM. The behavior of the Raman shift vs FWHM has been shown to follow a scaling law with parameter $\alpha \approx 1.55$, which corresponds well with previous claims of 1.5 for semiconductors like Si and GaAs.

Acknowledgment. We acknowledge the partial support of the New York State Science and Technology Foundation through its Centers for Advanced Technology Program. The authors S. Kelly and F. H. Pollak also acknowledge the partial support of U.S. Army Research Office Contract DAAHO4-94-G-0153.

References and Notes

(1) Gerischer, H.; Heller, A. *J. Phys. Chem*. **1991**, *95*, 5261.

(2) Gerischer, H.; Heller, A. *J. Electrochem. Soc*. **1992**, *139*, 113.

(3) Wang, C. M.; Heller, A.; Gerischer, H. *J. Am. Chem. Soc*. **1992**, *114*, 5230.

(4) Gerischer, H. *Electrochim. Acta* **1993**, *38*, 3.

(5) Brus, L. E. *J. Phys. Chem*. **1983**, *79*, 5566; **1984**, *80*, 4403.

(6) Tsu, R.; Ioriatti, L. *Superlattices Microstruct*. **1985**, *1*, 295.

(7) Höfler, H. J.; Hahn, H.; Averback, R. S. *Defect Diffus*. **1991**, *75*, 195.

(8) Dagan, G.; Tomkiewicz, M. *J. Phys. Chem*. **1993**, *97*, 12651.

(9) Tomkiewicz, M.; Kelly, S. *Fine Particles Science and Technology. From Micro to Nano particles*; Pelizzetti, E., Ed.; D. Reidel Publishing: Dordrecht, 1996.

(10) Zhu, Z.; Tsung, L. Y.; Tomkiewicz, M. *J. Phys. Chem*. **1995**, *99*, 15945, 15950.

(11) See for example: Brinker, C. J.; Scherer, G. W. *The Physics and Chemistry of Sol-Gel Processing*; Academic Press: New York, 1990.

(12) See for example: Pollak, F. H. *Analytical Raman Spectroscopy*; Grasselli, J. G., Bulkin, B. J., Eds.; John Wiley & Sons: New York, 1991; Chapter 6.

(13) Richter, H.; Wang, Z. P.; Ley, L. *Solid State Commun*. **1981**, *39*, 625.

(14) Zerda, T. W.; Hoang, G. *J. Non-Cryst. Solids* **1989**, *109*, 9.

(15) Doss, C. J.; Zallen, R. *Phys. Rev. B* **1993**, *48*, 15626.

(16) Hsu, L. S.; She, C. Y. *Opt. Lett*. **1985**, *10*, 638.

(17) Busca, G.; Ramis, G.; Gallardo Amores, J. M.; Escribano, V. S.; Plaggio, P. *J. Chem. Soc., Faraday Trans*. **1994**, *90*, 3181.

(18) Best, M. F.; Condrate, R. A., Sr. *J. Mater. Sci. Lett*. **1985**, *4*, 994−998.

(19) Berger, H.; Tang, H.; Lévy, F. *J. Cryst. Growth* **1993**, *130*, 108.

(20) Traylor, J. G.; Smith, H. G.; Nicklow, R. M.; Wilkinson, M. K. *Phys. Rev. B* **1971**, *3*, 3457.